Journal of Materials Chemistry C c9tc03987b

We have presented the Graphical Abstract text and image for your article below. This brief summary of your work will appear in the contents pages of the issue in which your article appears.

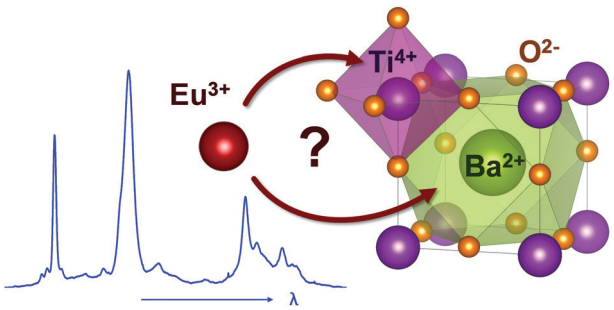

Site-selective symmetries of Eu^{3+}-doped $BaTiO_3$ ceramics: a structural elucidation by optical spectroscopy

Pablo Serna-Gallén, Héctor Beltrán-Mir, Eloísa Cordoncillo, Anthony R. West, Rolindes Balda and Joaquín Fernández

By means of optical spectroscopy, our study gives a plausible elucidation of Eu^{3+} site occupation in micron-sized $BaTiO_3$ particles.

Please check this proof carefully. Our staff will not read it in detail after you have returned it.

Please send your corrections either as a copy of the proof PDF with electronic notes attached or as a list of corrections. **Do not edit the text within the PDF or send a revised manuscript** as we will not be able to apply your corrections. Corrections at this stage should be minor and not involve extensive changes.

Proof corrections must be returned as a single set of corrections, approved by all co-authors. No further corrections can be made after you have submitted your proof corrections as we will publish your article online as soon as possible after they are received.

Please ensure that:

- The spelling and format of all author names and affiliations are checked carefully. You can check how we have identified the authors' first and last names in the researcher information table on the next page. **Names will be indexed and cited as shown on the proof, so these must be correct.**
- Any funding bodies have been acknowledged appropriately and included both in the paper and in the funder information table on the next page.
- All of the editor's queries are answered.
- Any necessary attachments, such as updated images or ESI files, are provided.

Translation errors can occur during conversion to typesetting systems so you need to read the whole proof. In particular please check tables, equations, numerical data, figures and graphics, and references carefully.

Please return your **final** corrections, where possible within **48 hours** of receipt, by e-mail to: materialsC@rsc.org. If you require more time, please notify us by email.

Funding information

Providing accurate funding information will enable us to help you comply with your funders' reporting mandates. Clear acknowledgement of funder support is an important consideration in funding evaluation and can increase your chances of securing funding in the future.

We work closely with Crossref to make your research discoverable through the Funding Data search tool (http://search.crossref.org/funding). Funding Data provides a reliable way to track the impact of the work that funders support. Accurate funder information will also help us (i) identify articles that are mandated to be deposited in **PubMed Central (PMC)** and deposit these on your behalf, and (ii) identify articles funded as part of the **CHORUS** initiative and display the Accepted Manuscript on our web site after an embargo period of 12 months.

Further information can be found on our webpage (http://rsc.li/funding-info).

What we do with funding information

We have combined the information you gave us on submission with the information in your acknowledgements. This will help ensure the funding information is as complete as possible and matches funders listed in the Crossref Funder Registry.

If a funding organisation you included in your acknowledgements or on submission of your article is not currently listed in the registry it will not appear in the table on this page. We can only deposit data if funders are already listed in the Crossref Funder Registry, but we will pass all funding information on to Crossref so that additional funders can be included in future.

Please check your funding information

The table below contains the information we will share with Crossref so that your article can be found *via* the Funding Data search tool. **Please check that the funder names and grant numbers in the table are correct and indicate if any changes are necessary to the Acknowledgements text.**

Funder name	Funder's main country of origin	Funder ID (for RSC use only)	Award/grant number
Universitat Jaume I	Spain	501100004834	Project UJI-B2016-38
Ministerio de Economía y Competitividad	Spain	501100003329	MAT2017-87035-C2-2-P
Euskal Herriko Unibertsitatea	Spain	501100003451	PPG17/07, GIU17/014

Q1

Researcher information

Please check that the researcher information in the table below is correct, including the spelling and formatting of all author names, and that the authors' first, middle and last names have been correctly identified. **Names will be indexed and cited as shown on the proof, so these must be correct.**

If any authors have ORCID or ResearcherID details that are not listed below, please provide these with your proof corrections. Please ensure that the ORCID and ResearcherID details listed below have been assigned to the correct author. Authors should have their own unique ORCID iD and should not use another researcher's, as errors will delay publication.

Please also update your account on our online manuscript submission system to add your ORCID details, which will then be automatically included in all future submissions. See here for step-by-step instructions and more information on author identifiers.

First (given) and middle name(s)	Last (family) name(s)	ResearcherID	ORCID iD
Pablo	Serna-Gallén		
Héctor	Beltrán-Mir		0000-0002-7836-1602
Eloísa	Cordoncillo		0000-0002-9368-1815
Anthony R.	West		
Rolindes	Balda		
Joaquín	Fernández		

Queries for the attention of the authors

Journal: **Journal of Materials Chemistry C**

Paper: **c9tc03987b**

Title: **Site-selective symmetries of Eu^{3+}-doped $BaTiO_3$ ceramics: a structural elucidation by optical spectroscopy**

For your information: You can cite this article before you receive notification of the page numbers by using the following format: (authors), J. Mater. Chem. C, (year), DOI: 10.1039/c9tc03987b.

Editor's queries are marked on your proof like this Q1, Q2, etc. and for your convenience line numbers are indicated like this 5, 10, 15, ...

Please ensure that all queries are answered when returning your proof corrections so that publication of your article is not delayed.

Query reference	Query	Remarks
Q1	Funder details have been incorporated in the funder table using information provided in the article text. Please check that the funder information in the table is correct.	
Q2	Please confirm that the spelling and format of all author names is correct. Names will be indexed and cited as shown on the proof, so these must be correct. No late corrections can be made.	
Q3	Do you wish to indicate the corresponding author(s)? If so, please specify the corresponding author(s).	
Q4	Do you wish to add an e-mail address for the corresponding author? If so, please provide the relevant information.	

Journal of Materials Chemistry C

PAPER

Site-selective symmetries of Eu^{3+}-doped $BaTiO_3$ ceramics: a structural elucidation by optical spectroscopy†

Cite this: DOI: 10.1039/c9tc03987b

Pablo Serna-Gallén,[a] Héctor Beltrán-Mir,[a] Eloísa Cordoncillo,[a] Anthony R. West,[b] Rolindes Balda[cde] and Joaquín Fernández[e]

Received 22nd July 2019,
Accepted 21st October 2019

DOI: 10.1039/c9tc03987b

rsc.li/materials-c

Eu^{3+}-Doped $BaTiO_3$ ceramics with dopant contents between 0 and 10 mol% were prepared by sol–gel synthesis based on the nominal compositions $(Ba_{1-3x}Eu_{2x})TiO_3$ and $Ba(Ti_{1-x}Eu_x)O_{3-x/2}$, where two possible substitution mechanisms are addressed. By means of optical spectroscopy, our study gives a plausible elucidation of Eu^{3+} site occupation in micron-sized $BaTiO_3$ particles. Time-resolved fluorescence line narrowing (TRFLN) shows the presence of five different crystal field sites for europium ions and possible symmetries are inferred for each one. The solubility limit of the lanthanide ion was found to be about 3 mol%. The experimental results are consistent with the preference of Eu^{3+} to occupy Ba^{2+} sites regardless of the nominal compositions and target substitution mechanism. However, TRFLN results reported that the dopant could also occupy Ti^{4+} sites, highlighting the amphoteric character of Eu^{3+}. The existence of anti-Stokes and Stokes vibronic sidebands in the $^5D_0 \rightarrow {}^7F_{0,1}$ transitions of Eu^{3+} ions is confirmed. This can explain the lack of resolution found in room temperature spectra of these transitions due to vibronic mixing of the excited levels. The existence of non-equivalent europium sites with different spectroscopic properties could have an impact on the optical properties of doped-$BaTiO_3$ ceramics and associated applications.

1. Introduction

Barium titanate, $BaTiO_3$, has been a longstanding material for electronic devices due to its broad spectrum of properties, such as spontaneous polarization, high dielectric permittivity in the paraelectric phase and piezoelectric response.[1] Luminescent trivalent lanthanide ions (Ln^{3+}) incorporated into solids have been greatly studied not only because of their application in emission displays and lasers but also for their ability to change and tune material properties depending on the site occupation of Ln^{3+} in the host lattice.[2] Indeed, Ln^{3+}-doped $BaTiO_3$ has shown outstanding performance in ferroelectric capacitors due to its high dielectric constant.[3]

Elucidating the distribution of Ln^{3+} involves determining if it occupies a single site (Ba^{2+} or Ti^{4+}) or multiple sites (both Ba^{2+} and Ti^{4+}), the solubility limit in each site, and how this distribution changes with lanthanide concentration.[4–7] According to different authors, the structural preference is for larger ions (La–Sm) to occupy the Ba^{2+} site while smaller ions (Yb, Lu) substitute onto the Ti^{4+} site. For intermediate-sized ions (Gd, Dy, Ho, Er), their amphoteric behaviour is highlighted; in other words, they are able to occupy both Ba^{2+} and Ti^{4+} positions.

Eu lies between Sm and Gd in the lanthanide series and therefore could show slight amphoteric character like Gd. Ba^{2+} has an ionic radius of 1.610 Å (for a 12 coordination number, CN), while Ti^{4+} has an ionic radius of 0.605 Å (for a CN = 6). Eu^{3+} has an intermediate radius of 0.947 Å (for a CN = 6) and 1.226 Å (for a CN = 12).[8,9] These values make it possible, in principle, for Eu^{3+} to occupy both sites.

However, there is still some controversy for Eu dopant distribution in the lattice. Based on X-ray diffraction (XRD) data, luminescence analysis and electrical measurements, some studies have proposed the presence of Eu in Ba^{2+} sites,[4,10] while others have concluded that Eu occupies both Ba^{2+} and Ti^{4+} sites.[4,9,11] Indeed, Rabuffetti *et al.*[4] also postulated that the mechanism of substitution could depend on Eu concentration: the results invoked the substitution of Eu^{3+} for

[a] Departamento de Química Inorgánica y Orgánica, Universidad Jaume I, Av. Sos Baynat s/n 12071, Castelló de la Plana, Spain
[b] Department of Materials Science & Engineering, University of Sheffield, Mappin Street, Sheffield S1 3JD, UK
[c] Departamento de Física Aplicada I, Escuela de Ingeniería de Bilbao, Universidad del País Vasco UPV-EHU, 48013 Bilbao, Spain
[d] Materials Physics Center CSIC-UPV/EHU, 20018 San Sebastian, Spain
[e] Donostia International Physics Center DIPC, 20018 San Sebastian, Spain

† Electronic supplementary information (ESI) available. See DOI: 10.1039/c9tc03987b

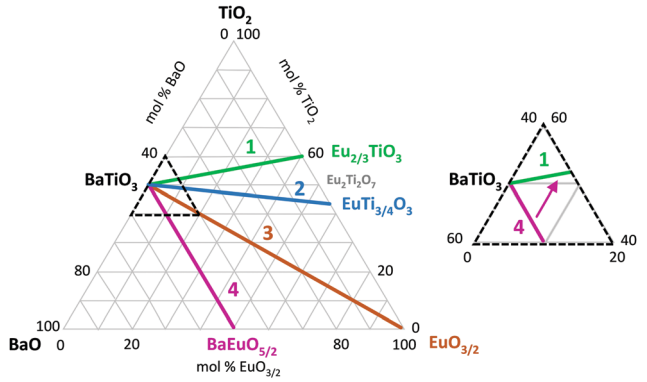

Fig. 1 A ternary composition triangle showing the location of possible ionic compensation mechanisms. The inset highlights a possible way of taking samples of join 4 towards join 1.

Ba^{2+} *via* creation of a Ti^{4+} vacancy at low doping concentrations (<1 mol%), and the substitution of Eu^{3+} for both Ba^{2+} and Ti^{4+} at high doping concentrations (1–3 mol%). Fig. 1 shows a ternary composition triangle, which highlights the different ionic compensation mechanisms that are possible and the location of the associated solid solutions as follows:

(1) $(Ba_{1-3x}Eu_{2x})TiO_3$, with creation of Ba^{2+} vacancies and Eu^{3+} occupying Ba^{2+} sites.

(2) $(Ba_{1-x}Eu_x)Ti_{1-x/4}O_3$, with creation of Ti^{4+} vacancies and Eu^{3+} occupying Ba^{2+} sites.

(3) $(Ba_{1-x}Ti_{1-x}Eu_{2x})O_3$, with double substitution of Eu^{3+} onto both Ba^{2+} and Ti^{4+} sites.

(4) $Ba(Ti_{1-x}Eu_x)O_{3-x/2}$, with creation of oxygen vacancies and Eu^{3+} occupying Ti^{4+} sites.

To the best of our knowledge, accurate studies to distinguish between these compensation mechanisms and associated defect structures have not been reported. In addition to these ionic compensation mechanisms, it is also important to consider possible electronic compensation mechanisms in which, depending on synthesis conditions, the valence state of Ti and/or Eu may vary.

The purposes of the present work are first, to determine which doping mechanism(s) is/are most likely under the synthesis conditions used and second, to measure the optical spectra of Eu-doped materials and correlate these with the probable defect structure and location of Eu^{3+} in the $BaTiO_3$ lattice. Samples were synthesised according to two possible mechanisms of substitution. The first one, addressed as the Ba-mechanism, has the nominal formula $(Ba_{1-3x}Eu_{2x})TiO_3$. This mechanism (1 in Fig. 1) has been reported for nanocrystals but not for micron-sized materials and implies that Eu^{3+} occupies only the Ba^{2+} site. It is well established that in nanomaterials the increasing number of surface and interface atoms generates stress/strain and concomitant structural perturbations which can affect local symmetries.[12] Thus, in our micron-sized compounds, there could be differences in the preference of Eu^{3+} for substitution sites. The second mechanism (4 in Fig. 1), referred to as the Ti-mechanism, has the nominal formula $Ba(Ti_{1-x}Eu_x)O_{3-x/2}$ and presumes that Eu^{3+} is present only in the Ti^{4+} site.

The site-resolved luminescence of Eu^{3+} in $BaTiO_3$ ceramics has been investigated, taking into account the adequacy of the dopant ion as a site-sensitive structural probe. Since the $^5D_0$ state is nondegenerate under any symmetry, the structure of the $^5D_0 \rightarrow {}^7F_J$ emission is determined only by the splitting of the terminal levels caused by the local crystal field. Moreover, as the $^7F_0$ level is also nondegenerate, site-selective excitation within the inhomogeneous broadened $^7F_0 \rightarrow {}^5D_0$ absorption band can be performed by using the fluorescence line-narrowing (FLN) technique to distinguish between different local environments around the lanthanide ions.[13–15]

2. Experimental section

2.1. Materials

Reagents used were barium acetate [$Ba(OAc)_2$ 99%], titanium(IV) isopropoxide [$Ti(OPr^i)_4$ 98%] and europium(III) acetate [$Eu(OAc)_3$ 99.9%] (Strem Chemicals), acetylacetone [acacH 99.8%] (Panreac), glacial acetic acid [HOAc 99.5%] (Labkerm) and methanol [MeOH 99.8%] (Scharlau).

2.2. Synthesis of Eu^{3+}-doped $BaTiO_3$ compounds

Samples with 0, 1, 2, 3, 4, 5 and 10 mol% Eu^{3+} content for each proposed mechanism (Ba or Ti-mechanism) were synthesised *via* the sol–gel method using the process reported previously:[16] barium acetate was dissolved in distilled water and europium acetate was added; methanol and acetic acid were then added to give clear solutions which were finally mixed with Ti^{4+}:acacH solution and left open in a desiccator to obtain clear gels. The molar ratios of reagents and solvents were $1Ba^{2+}$:$21H_2O$:40MeOH and $1Ti^{4+}$:8acacH. The dried gels were ground and the fine powders were fired at 1200 °C in air for two hours in Pt foil boats, obtaining micron-sized materials. To carry out optical analysis, pellets of the fired powders were made and sintered at 1200 °C in air for two hours in Pt foil boats. For convenience, the following abbreviations are used throughout the remainder of the article: "0%-BT" (for pure $BaTiO_3$), "*n*%-Ba" (for samples of the Ba-mechanism) and "*n*%-Ti" (for samples of the Ti-mechanism), where *n* takes the values of 1, 2, 3, 4, 5, and 10 and indicates the molar percentage of Eu^{3+} in the sample, Table 1.

2.3. Characterisation

Powder X-ray diffraction (XRD) measurements were performed using a Bruker D4-Endeavor X-ray diffractometer with CuK_α radiation at a scan speed of 0.3° min^{-1}. All data were collected between $15 \leq {}^\circ 2\theta \leq 70$ at room temperature. With the aim of calibrating peak positions, an internal standard of Si NIST (SRM 640e) was used. Lattice parameters were refined using the $WinX^{POW}$ 1.06 software version.

The microstructure of samples was observed using a JEOL 7001F scanning electronic microscope (SEM) equipped with a spectrometer for energy dispersive X-ray (EDX) analysis. The operation parameters were: acceleration voltage, 15 kV; measuring time, 20 s; and working distance, 10 mm.

This journal is © The Royal Society of Chemistry 2019

Table 1 Nominal compositions of the different synthesised samples in each mechanism and the abbreviations used

Mechanism	Reference	Nominal formula	x	Eu^{3+} mol%
	0%-BT	$BaTiO_3$	0	0
Ba-mechanism $(Ba_{1-3x}Eu_{2x})TiO_3$	1%-Ba	$(Ba_{0.985}Eu_{0.01})TiO_3$	0.005	1
	2%-Ba	$(Ba_{0.97}Eu_{0.02})TiO_3$	0.01	2
	3%-Ba	$(Ba_{0.955}Eu_{0.03})TiO_3$	0.015	3
	4%-Ba	$(Ba_{0.94}Eu_{0.04})TiO_3$	0.02	4
	5%-Ba	$(Ba_{0.925}Eu_{0.05})TiO_3$	0.025	5
	10%-Ba	$(Ba_{0.85}Eu_{0.10})TiO_3$	0.05	10
Ti-mechanism $Ba(Ti_{1-x}Eu_x)O_{3-x/2}$	1%-Ti	$Ba(Ti_{0.99}Eu_{0.01})O_{2.995}$	0.01	1
	2%-Ti	$Ba(Ti_{0.98}Eu_{0.02})O_{2.990}$	0.02	2
	3%-Ti	$Ba(Ti_{0.97}Eu_{0.03})O_{2.985}$	0.03	3
	4%-Ti	$Ba(Ti_{0.96}Eu_{0.04})O_{2.980}$	0.04	4
	5%-Ti	$Ba(Ti_{0.95}Eu_{0.05})O_{2.975}$	0.05	5
	10%-Ti	$Ba(Ti_{0.90}Eu_{0.10})O_{2.950}$	0.10	10

Different optical properties were studied for fired Eu^{3+}-doped $BaTiO_3$ samples. Emission measurements were performed at room temperature with an Eclipse Fluorescence Spectrophotometer (Varian). Spectra were recorded in the range 550–750 nm upon excitation at 466 nm (corresponding to the hypersensitive $^7F_0 \rightarrow {}^5D_2$ transition). From the spectra, the asymmetry ratio R (defined as the ratio between the intensities of $^5D_0 \rightarrow {}^7F_2$ and $^5D_0 \rightarrow {}^7F_1$ transitions) and the Ω_2 Judd–Ofelt parameter were calculated.

Resonant time-resolved FLN spectra were performed by exciting the samples with a pulsed frequency doubled Nd:YAG pumped tunable dye laser of 9 ns pulse width and 0.08 cm^{-1} linewidth and detected by an EGG&PAR Optical Multichannel Analyzer. The measurements were carried out at 10 K in a closed cycle helium cryostat.

3. Results and discussion

3.1. Structural characterisation

XRD patterns of the fired samples show all the peaks corresponding to the tetragonal phase of barium titanate (JCPDS-ICDD card 5-626), Fig. 2. No traces of crystalline secondary phases such as $Eu_2Ti_2O_7$ were detected apart from the presence of a secondary phase in the 10%-Ti sample, Fig. 2(b).

According to the ionic radius values, if Eu^{3+} occupies the Ba^{2+} site, there will be a contraction in the unit cell volume (V_0) while if it occupies the Ti^{4+} site, we expect an expansion in V_0.[17] Table 2 summarises the calculated lattice parameters; V_0 and tetragonality (c/a) ratios for the two composition series are shown in Fig. 3.

The evolution of V_0 and tetragonality with Eu^{3+} concentration has the same tendency. Therefore, further discussion focuses only on V_0. For the Ba-mechanism, there is a progressive decrease in V_0 up to 3 mol% of Eu^{3+} which is consistent with europium ions occupying the Ba^{2+} site. For concentrations $\geq$3 mol%, V_0 remains almost constant, suggesting that no more dopant enters the $BaTiO_3$ structure.

For samples of the Ti-mechanism, join 4, a progressive decrease in V_0 up to 2 mol%, is again observed highlighting the preference of europium for occupying the Ba^{2+} site.

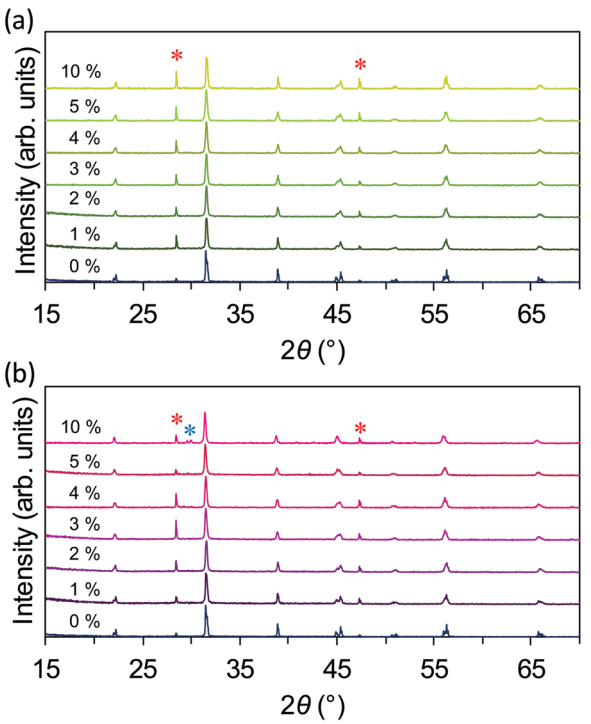

Fig. 2 XRD patterns for 0%-BT, (a) Ba-mechanism and (b) Ti-mechanism samples. The red stars point to the peaks corresponding to the internal standard of Si NIST (SRM 640e). The blue star highlights the presence of a secondary phase in the 10%-Ti sample.

However, the Ti-mechanism should lead to an increase in V_0 and not the observed decrease. We believe, therefore, that samples from the Ti-mechanism lost a small amount of BaO during high temperature firing, which had the effect of taking the samples towards join 1 or 3. Barium loss has been highly proved in the literature when doping perovskite-type structures with the general formula ABO_3.[18–27] This process has been attributed not only to the firing conditions but also to the dopant concentration. Indeed, the decreasing thermodynamic stability of the perovskite with increasing the amount of dopant implies a higher BaO activity and a greater thermodynamic driving force for Ba vaporization.[23] For yttrium-doped $BaZrO_3$, some studies have revealed the existence of BaO loss in a wide

Table 2 Unit cell parameters of Eu^{3+}-doped $BaTiO_3$ samples

Sample	a (Å)	c (Å)	V_0 (Å^3)	Sample	a (Å)	c (Å)	V_0 (Å^3)
0%-BT	3.9937(3)	4.0344(5)	64.347(7)	—	—	—	—
1%-Ba	3.9959(12)	4.0279(25)	64.313(21)	1%-Ti	3.9951(3)	4.0304(4)	64.329(6)
2%-Ba	3.9967(12)	4.0221(24)	64.247(17)	2%-Ti	3.9959(9)	4.0201(17)	64.19(3)
3%-Ba	3.9966(8)	4.0195(14)	64.202(10)	—	—	—	—
4%-Ba	3.9962(12)	4.0208(20)	64.212(15)	—	—	—	—
5%-Ba	3.9967(5)	4.0192(13)	64.202(16)	—	—	—	—
10%-Ba	3.9964(14)	4.0204(24)	64.212(18)	—	—	—	—

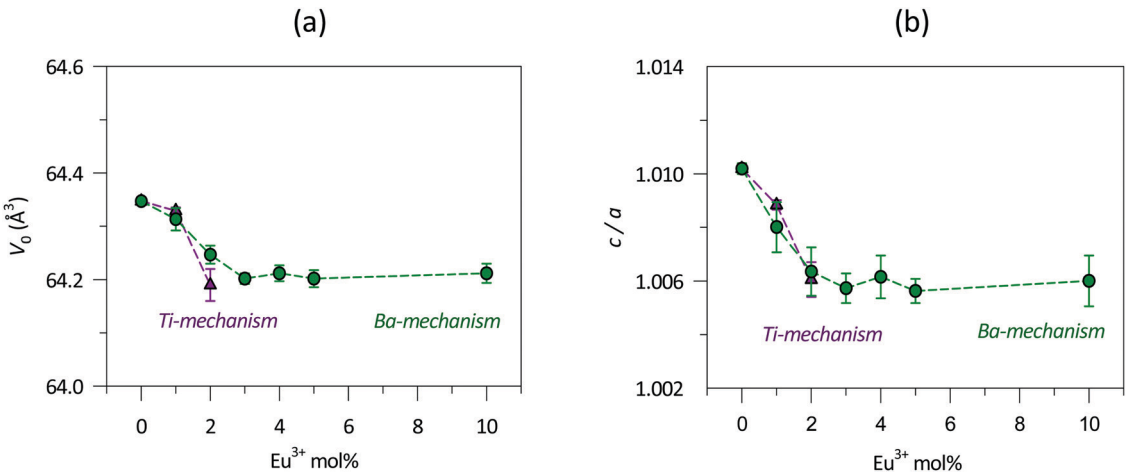

Fig. 3 Evolution of (a) V_0 and (b) c/a with Eu^{3+} concentration for Ba and Ti-mechanisms.

range of firing temperatures (1100–1600 °C).[18–20,23] The nominal composition of yttrium-doped barium zirconate is $Ba(Zr_{1-x}Y_x)O_{3-x/2}$, but the BaO loss implies that yttrium can have an amphoteric character, thus being able to occupy both A and B sites, and reaching the composition with the formula $(Ba_{1-x}Y_x)(Zr_{1-x}Y_x)O_3$. In a similar way, the same line of reasoning has been established for gadolinium-doped $BaCeO_3$ and computational studies have suggested that on energetic grounds, the site-occupancy of dopants is linked to barium loss.[22,25]

At higher Eu^{3+} contents on join 4, irregular lattice parameter results were obtained (not shown), consistent with some loss of Eu^{3+}, but not sufficient for the compositions to reach join 1. We conclude that there is little evidence for the Ti-mechanism of isolation with compositions on join 4, but do not discount the possibility of a double doping mechanism (join 3) in which Eu^{3+} is able to occupy both Ba^{2+} and Ti^{4+} sites simultaneously. Further work to investigate this possibility is in progress. Moreover, as previously explained, BaO loss is linked to the self-compensation mechanism. Indeed, the computational studies of Buscaglia *et al.*[28] revealed that for some Ln^{3+} ions (Tb^{3+}, Gd^{3+} and Er^{3+}), the self-compensation mechanism is the most probable. Considering this, the calculated lattice parameters would fit with join 3 as well.[19]

From the XRD results, we conclude that the solubility limit of Eu^{3+} in compositions with the Ba-mechanisms is ≈3 mol% (in agreement with some of the previously cited investigations[3,9]) and that europium has the preference for occupying the Ba^{2+} site. Fig. 4 shows as an example a SEM micrograph corresponding to the 2%-Ba fired sample, with micron-sized grains. For samples

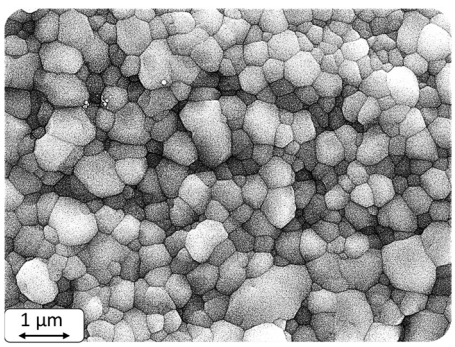

Fig. 4 SEM micrograph of the 2%-Ba fired sample.

with a higher content of Eu^{3+}, SEM/EDX analysis of the powders revealed the presence of europium-rich rod-like particles that could be attributed to secondary phases not detected by XRD (see Fig. S1 of the ESI†). There is no evidence for significant doping by the Ti-mechanism, but the possibility exists for a certain amount of double doping.

3.2. Luminescence studies at room temperature

Optical characterisation at room temperature was carried out for samples with Eu^{3+} content ≤4 mol% for the Ba-mechanism and ≤2 mol% for the Ti-mechanism. Room temperature emission spectra of the fired samples are shown in Fig. 5, where the emission bands are assigned to the following transitions[29]: $^5D_0 \rightarrow {}^7F_0$ (580 nm), $^5D_0 \rightarrow {}^7F_1$ (596 nm), $^5D_0 \rightarrow {}^7F_2$

 This journal is © The Royal Society of Chemistry 2019

(616 nm), $^5D_0 \rightarrow {}^7F_3$ (645–660 nm) and $^5D_0 \rightarrow {}^7F_4$ (680–715 nm), Fig. 5(a). Spectra were collected upon excitation at the hypersensitive $^7F_0 \rightarrow {}^5D_2$ transition (466 nm) and were normalised to the magnetic dipole $^5D_0 \rightarrow {}^7F_1$ transition.

As pointed out in the literature,[30,31] the Ω_2 Judd–Ofelt parameter correlates with the polarizable and covalent character of the lanthanide ion in the lattice. Thus, the study of this parameter could shed light on the Eu^{3+} surroundings in the host lattice. According to Judd–Ofelt theory, the emission rate of a transition $i \rightarrow j$ can be expressed as:

$$A_{ij} = \frac{64e^2\pi^4}{3h\lambda_{ij}^3} \cdot \frac{\chi}{(2J+1)} \cdot \sum_{\lambda=2,4,6} \Omega_\lambda \left\| U^\lambda \right\| \quad (1)$$

where λ_{ij} is the average wavelength of the transition $i \rightarrow j$; Ω_λ is the Judd–Ofelt parameter; $\|U^\lambda\|$ is an abbreviation of $|\langle \|U^\lambda\| \rangle|^2$, which corresponds to the reduced matrix elements of the unit tensor operator connecting states i and j; χ is the Lorentz local field correction term (which is equal to $\frac{n(n^2+2)^2}{9}$, n is the refractive index at λ_{ij}); e is the elementary charge; h is the Planck constant; and J refers to state i.[32]

From the experimental emission spectra, A_{0J} can be calculated using the expression:

$$A_{0J} = A_{01} \cdot \frac{I_{0J}}{I_{01}} \cdot \frac{\lambda_{0J}}{\lambda_{01}} \quad (2)$$

where A_{01} is the magnetic dipole transition rate assumed constant and equal to 50 s^{-1}; I and λ are the intensity and the wavelength value of the transition $0 \rightarrow J$, respectively.

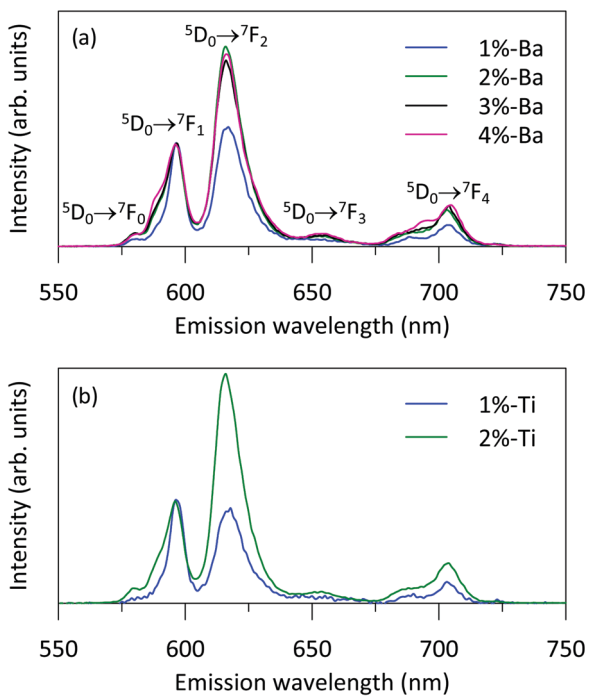

Fig. 5 Room temperature emission spectra corresponding to the $^5D_0 \rightarrow {}^7F_{0-4}$ transitions of (a) Ba-mechanism and (b) Ti-mechanism samples upon excitation at 466 nm.

A combination of expressions (1) and (2) for the $^5D_0 \rightarrow {}^7F_2$ transition results in:

$$\Omega_2 = A_{01} \cdot \frac{I_{02}}{I_{01}} \cdot \frac{{\lambda_{02}}^4}{\lambda_{01}} \cdot \frac{3h}{64e^2\pi^4\chi\|U^2\|} \quad (3)$$

The asymmetry ratio R between the intensities of $^5D_0 \rightarrow {}^7F_2$ and $^5D_0 \rightarrow {}^7F_1$ transitions is defined as:

$$R = \frac{I_{02}}{I_{01}} \quad (4)$$

Thereby, we can rewrite expression (3) as follows:

$$\Omega_2 = A_{01} \cdot R \cdot \frac{{\lambda_{02}}^4}{\lambda_{01}} \cdot \frac{3h}{64e^2\pi^4\chi\|U^2\|} \quad (5)$$

The value reported in the literature for $\|U^2\|$ is 0.0032.[33] The average wavelength value obtained for samples is 596 nm for λ_{01}($^5D_0 \rightarrow {}^7F_1$ transition) and 616 nm for λ_{02} ($^5D_0 \rightarrow {}^7F_2$ transition). The refractive index of $BaTiO_3$ at 616 nm is 2.4122.[34] Expressing λ_{0J} in cm, taking $h = 6.6261 \times 10^{-27}$ erg s, $e = 4.803 \times 10^{-10}$ esu[35] and substituting the rest of values, Ω_2 can be expressed as:

$$\Omega_2 = (3.1844R) \times 10^{-21}\ \text{cm}^2 \quad (6)$$

Higher values of Ω_2 suggest that the environment around europium in the $BaTiO_3$ structure is more polarizable and covalent.[30] The ionic radius and CN for Ba^{2+} are higher than for Ti^{4+}. In this way, there will be more electronic distortion around Eu^{3+} in the Ba^{2+} site, which means that the ion is more polarizable. Therefore, higher values of Ω_2 are expected if the majority of Eu^{3+} ions occupy Ba^{2+} sites. R and Ω_2 values are summarised in Table 3 for samples of both mechanisms; Ω_2 evolution with Eu^{3+} concentration is plotted in Fig. 6.

From the analysis of Ω_2 evolution with Eu^{3+} content, similar conclusions to the ones obtained by XRD can be drawn. For Ba-mechanism samples, Ω_2 increases until a concentration of 2 mol% Eu^{3+}. Then, the Judd–Ofelt parameter remains nearly constant, implying there are no noticeable changes in the polarizability environment of the ion, an aspect closely related to the solubility limit. Ti-mechanism samples follow the same tendency up to 2 mol% Eu^{3+}. Therefore, the crystal field of Eu^{3+} must be quite similar, suggesting that europium occupies the same substitution sites. Linking these results to those of XRD analysis, we conclude that the preference of Eu^{3+} is to occupy the Ba^{2+} site up to 2%, regardless of the nominal composition of the mechanism postulated.

Table 3 R and Ω_2 values obtained from emission spectra at room temperature (λ_{exc} = 466 nm)

Sample	R	Ω_2 (10^{-21} cm^2)	Sample	R	Ω_2 (10^{-21} cm^2)
1%-Ba	1.17	3.73(3)	1%-Ti	0.93	2.96(2)
2%-Ba	1.95	6.21(5)	2%-Ti	2.24	7.13(6)
3%-Ba	1.82	5.80(4)	—	—	—
4%-Ba	1.88	5.99(5)	—	—	—

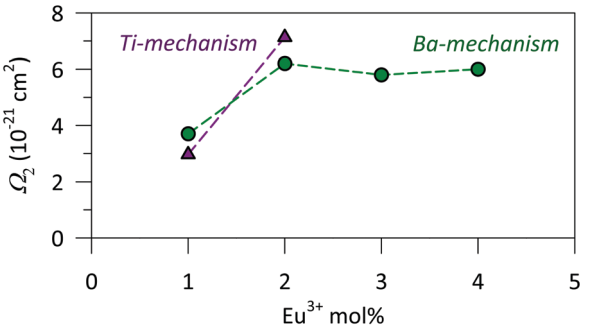

Fig. 6 Ω_2 evolution with Eu^{3+} concentration for samples on Ba and Ti-mechanism joins.

3.3. FLN spectra

3.3.1. Experimental results. Low temperature site-selective excitation of Eu^{3+}, performed by using the time-resolved fluorescence line-narrowing (TRFLN) technique in cation-defective $BaTiO_3$ samples, displayed complex behaviour which points to the existence of at least five different crystal field sites for the lanthanide ion. In order to simplify the description of the different sites and following the standard acronym ABX_3 to describe perovskite oxides, we call A_i and B_i the lanthanide substitutional centres in the $BaTiO_3$ matrix when Eu^{3+} occupies Ba^{2+} and Ti^{4+} sites, respectively.

Fig. 7 shows a selection of low temperature (10 K) TRFLN spectra corresponding to the $^5D_0 \rightarrow {}^7F_{0-2}$ transitions of 1%-Ba obtained with a time delay of 10 μs after the pump pulse (~0.08 cm^{-1} spectral width) at three different pumping wavelengths within the $^7F_0 \rightarrow {}^5D_0$ transition. Depending on the excitation wavelength, the emission spectra present different characteristics regarding the number of observed $^5D_0 \rightarrow {}^7F_J$ components, their relative intensity, and the magnitude of the observed crystal-field splitting for each ^7F_J state.

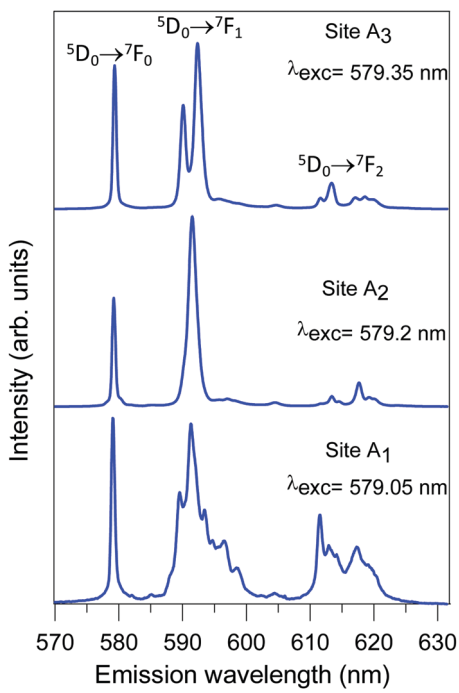

Fig. 7 Low temperature (10 K) TRFLN spectra corresponding to the $^5D_0 \rightarrow {}^7F_{0-2}$ transitions of the 1%-Ba sample obtained with a time delay of 10 μs after the pump pulse at three different pumping wavelengths.

Starting from the bottom of Fig. 7, the 1%-Ba (site A_1) spectrum obtained by pumping at 579.05 nm displays, besides the single component of the resonant $^5D_0 \rightarrow {}^7F_0$ emission, a three-component emission corresponding to the $^5D_0 \rightarrow {}^7F_1$ magnetic dipole transition and a weaker multiple peak emission from the $^5D_0 \rightarrow {}^7F_2$ electric dipole emission. The strong intensity of the $^5D_0 \rightarrow {}^7F_0$ emission suggests the presence of large linear terms in the crystal field potential. The 1%-Ba (site A_2) spectrum measured by pumping at 579.20 nm exhibits a single $^5D_0 \rightarrow {}^7F_1$ emission peak with the highest intensity among all the observed $^5D_0 \rightarrow {}^7F_J$ transitions with a weak contribution from the electric dipole $^5D_0 \rightarrow {}^7F_2$ emission. Finally, the 1%-Ba (site A_3) spectrum obtained by exciting at 579.35 nm shows a prominent $^5D_0 \rightarrow {}^7F_0$ resonance emission together with a two-component $^5D_0 \rightarrow {}^7F_1$ emission accompanied by a weak $^5D_0 \rightarrow {}^7F_2$ contribution. The wavelengths of the $^5D_0 \rightarrow {}^7F_J$ ($J = 0, 1, 2, 3, 4$) emission peaks for the three sites are provided in Table S1 (ESI†).

The spectra of the 2%-Ba and (1,2)%-Ti samples (not shown) indicated no significant differences for the three A_1, A_2 and A_3 sites (pumping wavelengths and emission intensities) as compared to those in the 1%-Ba sample. They showed similar emission sites but noting that with the increase of Eu^{3+}doping, the emission efficiency of Site A_1 increased (it was more sharply defined), whereas A_2 and A_3 sites were not much affected.

However, the spectral behaviour of 3%-Ba and 3%-Ti samples, displayed in Fig. 8, exhibits significant changes in the crystal field around the lanthanide ions. In particular, site A_1 disappears in the 3%-Ti sample whereas a new one, site B_1, appears at longer wavelengths and another one, site B_2, (red stars in Fig. 8) clearly emerges at the long wavelength tail of the $^5D_0 \rightarrow {}^7F_1$ emissions of main site A_2 and site A_3. This new site, which also weakly appears (less pronounced) in the 3%-Ba sample, has the longest lifetime of all the observed emissions as we shall next see.

In conclusion, we found three A-type and two B-type crystal field sites for Eu^{3+}, summarised in Table 4, whose symmetry is discussed below.

3.3.2. On the origin and symmetries of the Eu^{3+}sites in barium titanate. Possible origins of spectral differences associated with doped powder samples are as follows: First, lattice deformations near grain surfaces may produce variable Ln^{3+} environments even though the Ln^{3+} ions occupy similar substitutional sites. Consequently, different crystal field sites and/or glass-like disorder may be observed in the Ln^{3+} emission spectrum. Second, at low temperature (10 K) in the rhombohedral phase of $BaTiO_3$, we expect the presence of defects to compensate the excess of charge introduced by the Ln^{3+} ion. This may lead to a symmetry lowering at the substitutional site from the cubic symmetry class at high temperature.[36] EPR studies on Gd^{3+}-doped $BaTiO_3$ (both $Eu^{3+}$and Gd^{3+} have similar

This journal is © The Royal Society of Chemistry 2019

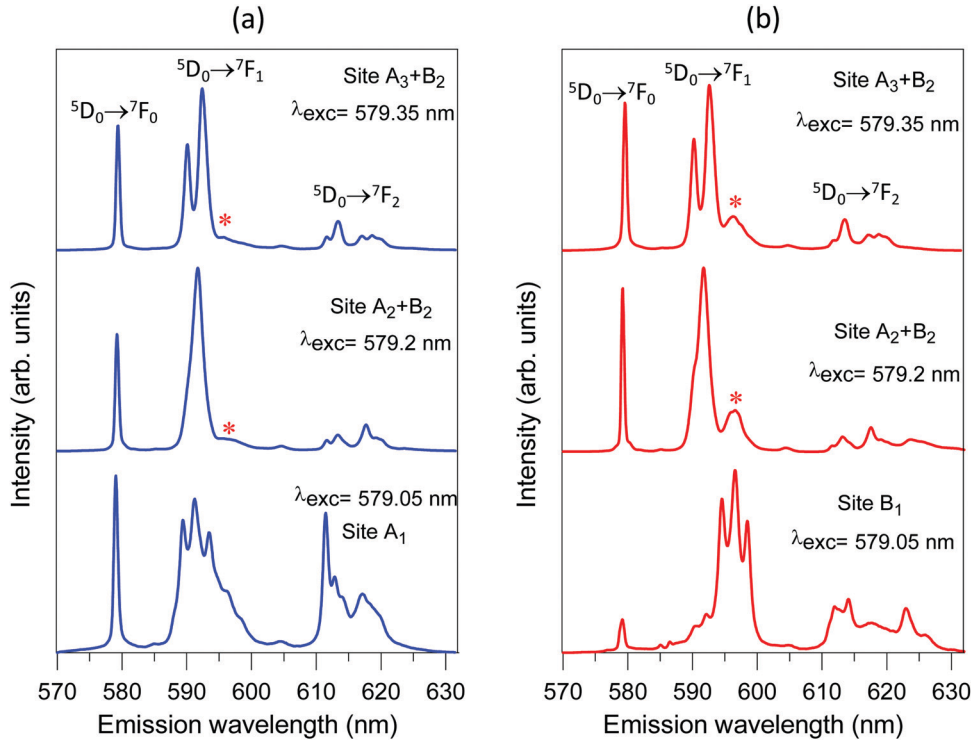

Fig. 8 Low temperature (10 K) TRFLN $^5D_0 \rightarrow {}^7F_{0-2}$ emission spectra of samples (a) 3%-Ba and (b) 3%-Ti showing the emissions from sites A_1, A_2, A_3, B_1, and B_2 (red stars).

Table 4 Description of the different crystal field sites for Eu^{3+} ions in doped-$BaTiO_3$ samples. The abbreviations A_i and B_i refer to Eu^{3+} occupying Ba^{2+} and Ti^{4+} sites, respectively

λ_{exc} (nm)	Site	Symmetry
579.05	A_1	Low (near particle surface)
	B_1	Low (near particle surface)
579.20	A_2	Close to cubic
	B_2	Cubic (O_h)
579.35[a]	A_3	Trigonal (C_{3v} or C_3)

[a] The emission of Site B_2 can also be observed when pumping at 579.35 nm due to vibronic coupling.

ionic radii) showed that Gd substituted the alkali earth ion with no remarkable distortion effects.[37] For Eu-doped barium titanate prepared by the sol–gel method, the presence of glassy-like spectral disorder when exciting at a direct Ln^{3+} level has been noted previously,[38,39] although only a few discuss the possibility of double substitution of Eu onto both Ba and Ti.[4,9,40]

The low-temperature time-resolved emission spectra, Fig. 8, show the existence of low symmetry sites: A_1 and B_1. Site A_1 could be related to Eu^{3+} ions occupying a substitutional Ba^{2+} site in a highly distorted environment in a thin shell near the grain surfaces, whereas B_1, with a similar $^5D_0 \rightarrow {}^7F_1$ emission, but appearing at longer wavelengths, could be associated with Eu^{3+} occupancy of a distorted Ti^{4+} site;[41] distorted sites near particle surfaces have been observed in other Eu^{3+}-doped oxide powders.[42] The TRFLN spectra display nearly equal intensities for the $^5D_0 \rightarrow {}^7F_0$, $^5D_0 \rightarrow {}^7F_1$ and $^5D_0 \rightarrow {}^7F_2$ transitions with one, three, and five peaks, respectively, as well as an intense $^5D_0 \rightarrow {}^7F_4$ transition (see Fig. S2(a) in the ESI†), which are compatible with a C_s, C_2, or C_1 point symmetries. However, site A_2 shows the most intense and single component $^5D_0 \rightarrow {}^7F_1$ emission, with a very small contribution from the electric dipole $^5D_0 \rightarrow {}^7F_2$ transition, which suggests a high symmetry, anion distribution around Eu^{3+}. This is consistent with the expectation that the high coordination number of Ba^{2+} (CN = 12) tends to increase the effective site symmetry which reduces and/or suppresses crystal field splitting. Although the presence of a strong $^5D_0 \rightarrow {}^7F_0$ peak and several $^5D_0 \rightarrow {}^7F_4$ emission components (see Fig. S2(b), ESI†) excludes formal cubic point symmetry at site A_2, nevertheless, as pointed out in ref. 36, low-temperature rhombohedral $BaTiO_3$ has symmetry close to that of high-temperature cubic $BaTiO_3$ and therefore, the point symmetry of site A_2 is close to cubic. However, the presence of the $^5D_0 \rightarrow {}^7F_4$ emission implies a cubic distortion enough to supress the center of symmetry.[37]

Referring to site A_3, the FLN spectra in Fig. 8 show two-component emission for the $^5D_0 \rightarrow {}^7F_1$ transition and five $^5D_0 \rightarrow {}^7F_4$ components (see Fig. S2(c), ESI†); this result is compatible with a C_{3v} point group symmetry.[29] We notice that the bump appearing at the long wavelength tail of the $^5D_0 \rightarrow {}^7F_1$ emission in both A_2 and A_3 sites (marked with a red star) corresponds to site B_2 discussed below.

The luminescence decays of the different Eu^{3+} sites are hard to measure due to the tight excitation bandwidth of the three sites and the spectral overlap of the emission components. Therefore, we have only measured the lifetime of the main site A_2 by integrating the time resolved $^5D_0 \rightarrow {}^7F_0$ emission of the

3%-Ba sample. The result is a non-exponential decay with a bi-exponential character. The long and short-lived components are about 3 ms and 300 μs, respectively. This result agrees with former lifetime measurements in Eu-doped $BaTiO_3$[38] reinforcing the hypothesis about the existence of non-inversion symmetry sites (A_1, A_3, B_1) giving rise to a short lifetime component as well as near centrosymmetric ones (A_2) carrying the long lived one.

Fig. 9 displays the time-resolved spectra corresponding to the $^5D_0 \rightarrow {}^7F_{0-2}$ emissions of both 3%-Ba and 3%-Ti samples excited at 579.20 nm, the wavelength used for exciting site A_2. As time evolves, the main features of site A_2 disappear whereas the bump at the low energy side of the $^5D_0 \rightarrow {}^7F_1$ emission peak grows and becomes the only remaining spectral component at 596.9 nm. The lifetime of this component is longer than 12 ms, the temporal range of our optical multichannel analyser. This weak emission would thus correspond to the new Eu^{3+} crystal field site B_2 discussed above. The absence of other spectral components, including the $^5D_0 \rightarrow {}^7F_0$ emission, points to cubic point symmetry for this site.

As Fig. 8 shows, the emission of site B_2 is also observed when pumping site A_3 at 579.35 nm, which suggests the presence of strong vibronic coupling that allows the cubic site to be pumped through the vibronic sidebands of the electronic level. In good agreement with this observation, our FLN measurements confirm the presence of anti-Stokes and Stokes vibronic sidebands in the $^5D_0 \rightarrow {}^7F_0$ (peaking at around 38 and 63 cm^{-1} from the $^5D_0 \rightarrow {}^7F_0$ main peak at 17265 cm^{-1}) and $^5D_0 \rightarrow {}^7F_1$ (anti-Stokes at 119 and Stokes at 146 cm^{-1} vibronic sidebands) transitions. As an example, Fig. 10 shows the emission of site A_2 by pumping its anti-Stokes vibronic band at 577.9 nm in the 1%-Ba sample. These broad vibronic bands, together with inherent disorder introduced by charge compensation, promote the observed glass-like disorder when not pumping at the precise wavelength of the electronic transition.

When considering the possible charge compensation mechanisms associated with Ln^{3+} doping, different possibilities are indicated in Fig. 1. Oxygen vacancies are not expected to play a significant role, as first the samples were sintered in air and second, there was no evidence for doping on join 4, Fig. 1. The plausible mechanisms are therefore close to those proposed in ref. 4, 9 and 40 in which the existence of europium sites A assuming Ti^{4+} vacancies or a self-compensation mechanism produced by Eu^{3+} pairs substituting Ba^{2+} and Ti^{4+} crystal sites (mechanisms 2 and 3 of Fig. 1) is suggested.

We shall first focus on the main A_2 site, disregarding the low crystal field symmetry of A_1 and B_1 sites due to the lattice deformation near the particle surface. In spite of the smaller ionic radius of Eu^{3+} (r_{Eu} = 1.226 Å with CN = 12) if compared with the one of Ba^{2+} (r_{Ba} = 1.610 Å), the apparent high symmetry of this site is only compatible with a very low distorted oxygen coordination, meaning that the unit cell centered at the Ln^{3+} ion could be neither titanium defective nor self-compensated by a Ln_{Ba} + Ln_{Ti} pair.[9,40]

This result suggests that the compensation mechanism would be located in cells neighboring the defect carrier. But

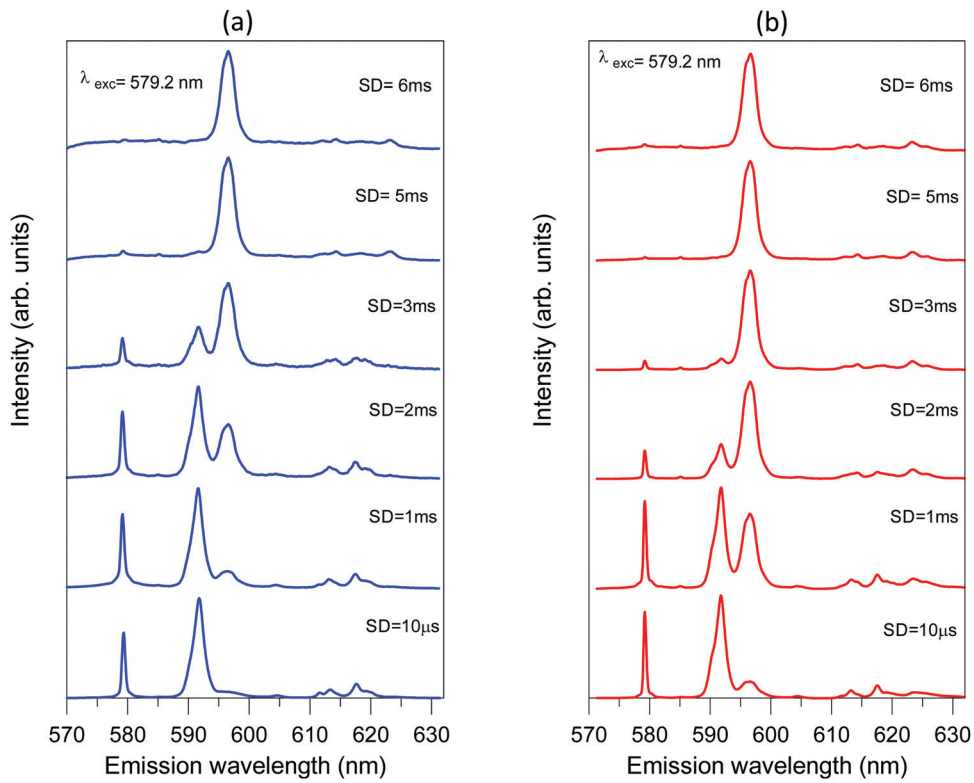

Fig. 9 Time-resolved $^5D_0 \rightarrow {}^7F_{0-2}$ emission spectra of A_2 + B_2 sites in both (a) 3%-Ba and (b) 3%-Ti samples excited at 579.20 nm.

This journal is © The Royal Society of Chemistry 2019

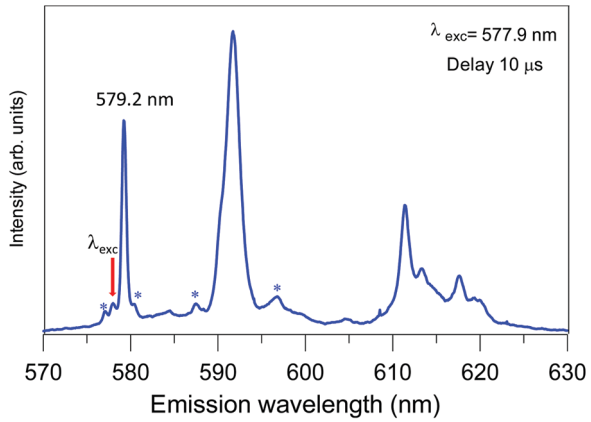

Fig. 10 $^5D_0 \rightarrow {}^7F_{0-2}$ emission spectrum of site A_2 by pumping its anti-Stokes vibronic band at 577.9 nm in the 1%-Ba sample. The stars point to the vibronic components of the $^5D_0 \rightarrow {}^7F_{0-1}$ transitions.

in the case where the unit cell would present a Ti^{4+} vacancy and/or a substitutional Eu^{3+} pair, it would be still possible to keep a trigonal axis of symmetry along the Ln–Ln or Ln–Ti (vacancy) diagonal of the unit cell which would lower the symmetry to C_{3v} or C_3, giving rise to the observed symmetry of site A_3.

Referring to site B_2, its features are only compatible with a high symmetry octahedral crystal field site associated with the Ti^{4+}substitution by Eu^{3+}. As the octahedral coordinated ionic radius of Eu^{3+} (0.947 Å) is higher than the one of Ti^{4+} (0.605 Å), we expect a stronger cation–anion interaction giving rise to a highly symmetric crystal field around the Eu^{3+} ion. Moreover, the stronger Eu–O interaction at the Ti^{4+} site, if compared with the one at site Ba^{2+}, makes potential energy curves of Eu^{3+} centers to become steeper at the Ti^{4+} sites if compared to those of Eu^{3+}at Ba^{2+}sites, giving rise to the observed red-shift of the Eu^{3+}emission bands at the Ti^{4+} sites.

4. Conclusions

The crystallographic nature and spectroscopic properties of non-equivalent europium sites in $BaTiO_3$ have been investigated. The samples were synthesised *via* the sol–gel method in accordance with the nominal formula of two possible substitution mechanisms: $(Ba_{1-3x}Eu_{2x})TiO_3$ and $Ba(Ti_{1-x}Eu_x)O_{3-x/2}$. Bearing in mind the adequacy of the dopant ion as a structural probe, site-selective excitation within the inhomogeneous broadened $^7F_0 \rightarrow {}^5D_0$ absorption band was performed. The obtained results allow us to draw the following conclusions:

• The solubility limit of Eu^{3+} in $BaTiO_3$ samples has been found to be 3 mol%.

• The preference of Eu^{3+} is to occupy Ba^{2+} sites regardless of the nominal compositions and substitution mechanism. The main luminescence emission can be attributed to Eu^{3+} occupying Ba^{2+} substitutional sites; in particular, site A_2 is the most efficient emitter. Besides, Ti^{4+} site occupancy has also been proved by their FLN emission.

• XRD data and Ω_2 Judd–Ofelt parameters are in agreement with the site-selective excitation results. TRFLN spectra show the presence of five different europium crystal field sites and possible crystal symmetries have been inferred for each one.

• TRFLN measurements confirm the presence of relatively strong anti-Stokes and Stokes vibronic sidebands in the $^5D_0 \rightarrow {}^7F_{0,1}$ transitions. This important issue can explain the lack of site resolution found in the room temperature spectra of these transitions, obtained by selective pumping of the hypersensitive $^5D_2$ level, due to the vibronic mixing of the excited levels.

This study highlights the amphoteric behaviour of Eu^{3+} in $BaTiO_3$, but with the proviso that mainly substitution occurs in the Ba site. As has been reported in the literature,[3] noticeable changes for both electric and magnetic properties of the material are observed depending on the site occupancy of dopants. Therefore, the presence of different crystallographic sites for Eu^{3+} could have a decisive impact not only on the optical properties of $BaTiO_3$ ceramics but also on their wide range of electronic properties and device applications.

Conflicts of interest

There are no conflicts to declare.

Acknowledgements

P. S.-G., H. B.-M. and E. C. thank the Universidad Jaume I (Project UJI-B2016-38) and Ministerio de Economía y Empresa (Project MAT2016-80410-P) for financial support. P. S.-G. also thanks Universidad Jaume I for a fellowship. R. B. and J. F. acknowledge financial support from MINECO under Project MAT2017-87035-C2-2-P (AEI/FEDER, UE), Basque Country University PPG17/07 and GIU17/014, and Basque Country Government PIBA2018-24.

References

1 D. Sitko, *Phase Transitions*, 2014, **87**, 1002–1010.
2 J. R. Miranda, A. G. Murillo, F. D. J. C. Romo, J. O. Uc, C. A. Fl. Sandoval, A. D. J. M. Ramírez, S. Velumani, E. de la Rosa Cruz and V. G. Febles, *J. Sol–Gel Sci. Technol.*, 2014, **72**, 435–442.
3 A. Ahad, M. A. Taher, M. K. Das, M. Z. Rahaman and M. N. I. Khan, *Results Phys.*, 2019, **12**, 1925–1932.
4 F. A. Rabuffetti, S. P. Culver, J. S. Lee and R. L. Brutchey, *Nanoscale*, 2014, **6**, 2909–2914.
5 T. D. Dunbar, W. L. Warren, B. A. Tuttle, C. A. Randall and Y. Tsur, *J. Phys. Chem. B*, 2004, **108**, 908–917.
6 L. A. Xue, Y. Chen and R. J. Brook, *Mater. Sci. Eng., B*, 1988, **1**, 193–201.
7 M. T. Buscaglia, V. Buscaglia, P. Ghigna, M. Viviani, G. Spinolo, A. Testino and P. Nanni, *Phys. Chem. Chem. Phys.*, 2004, **6**, 3710–3713.
8 R. D. Shannon, *Acta Crystallogr., Sect. A: Cryst. Phys., Diffr., Theor. Gen. Crystallogr.*, 1976, **A32**, 751–767.
9 D. Y. Lu, T. Ogata, H. Unuma, X. C. Li, N. N. Li and X. Y. Sun, *Solid State Ionics*, 2011, **201**, 6–10.

10 M. K. Rath, G. K. Pradhan, B. Pandey, H. C. Verma, B. K. Roul and S. Anand, *Mater. Lett.*, 2008, **62**, 2136–2139.
11 D.-Y. Lu, T. Koda, S. Hideshige and M. Toda, *J. Ceram. Soc. Jpn.*, 2005, **113**, 721–727.
12 B. Cojocaru, D. Avram, V. Kessler, V. Parvulescu, G. Seisenbaeva and C. Tiseanu, *Sci. Rep.*, 2017, **7**, 1–14.
13 C. Cascales, R. Balda, V. Jubera, J. P. Chaminade and J. Fernández, *Opt. Express*, 2008, **16**, 2653–2662.
14 C. Cascales, P. Porcher, J. Fernández, A. Oleaga, R. Balda and E. Diéguez, *J. Alloys Compd.*, 2001, **323–324**, 260–266.
15 C. Cascales, J. Fernández and R. Balda, *Opt. Express*, 2005, **13**, 2141–2152.
16 H. Beltrán, E. Cordoncillo, P. Escribano, D. C. Sinclair and A. R. West, *J. Am. Ceram. Soc.*, 2004, **87**, 2132–2134.
17 Y. Tsur, T. D. Dunbar and C. A. Randall, *J. Electroceram.*, 2001, **7**, 25–34.
18 E. Fabbri, D. Pergolesi, S. Licoccia and E. Traversa, *Solid State Ionics*, 2010, **181**, 1043–1051.
19 Y. Yamazaki, C.-K. Yang and S. M. Haile, *Scr. Mater.*, 2011, **65**, 102–107.
20 Y. Yamazaki, R. Hernandez-Sanchez and S. M. Haile, *J. Mater. Chem.*, 2010, **20**, 8158–8166.
21 T. Ogihara, H. Aikiyo, N. Ogata and N. Mizutani, *Adv. Powder Technol.*, 1999, **10**, 37–50.
22 D. Shima and S. M. Haile, *Solid State Ionics*, 1997, **97**, 443–455.
23 M. D. Gonçalves, P. S. Maram, R. Muccillo and A. Navrotsky, *J. Mater. Chem. A*, 2014, **2**, 17840–17847.
24 J.-S. Chun, N.-M. Hwang, D.-Y. Kim and J.-K. Park, *J. Am. Ceram. Soc.*, 2004, **87**, 1779–1781.
25 J. Wu, R. A. Davies, M. S. Islam and S. M. Haile, *Chem. Mater.*, 2005, **17**, 846–851.
26 S. Imashuku, T. Uda, Y. Nose, G. Taniguchi, Y. Ito and Y. Awakura, *J. Electrochem. Soc.*, 2009, **156**, 1–8.
27 I. Antunes, S. Mikhalev, G. C. Mather, V. V. Kharton, F. G. Figueiras, A. Alves, J. Rodrigues, M. R. Correia, J. R. Frade and D. P. Fagg, *Inorg. Chem.*, 2016, **55**, 8552–8563.
28 M. T. Buscaglia, V. Buscaglia, M. Viviani and P. Nanni, *J. Am. Ceram. Soc.*, 2001, **84**, 376–384.
29 K. Binnemans, *Coord. Chem. Rev.*, 2015, **295**, 1–45.
30 D. K. Patel, B. Vishwanadh, V. Sudarsan and S. K. Kulshreshtha, *J. Am. Ceram. Soc.*, 2013, **96**, 3857–3861.
31 C. de Mello Donegá, S. A. Junior and G. F. de Sá, *J. Alloys Compd.*, 1997, **250**, 422–426.
32 B. Julián, J. Planelles, E. Cordoncillo, P. Escribano, P. Aschehoug, C. Sanchez, B. Viana and F. Pellé, *J. Mater. Chem.*, 2006, **16**, 4612–4618.
33 S. Constantin and M. L. Stanciu, *Ann. West Univ. Timisoara - Phys.*, 2012, **56**, 127–131.
34 M. N. Polyanskiy, Refractive index database, https://refractiveindex.info, accessed 23 April 2018.
35 Y. H. Elbashar and D. A. Rayan, *Int. J. Appl. Chem.*, 2016, **12**, 59–66.
36 H. Yamamoto, S. Makishima and S. Shionoya, *J. Phys. Soc. Jpn.*, 1967, **23**, 1321–1332.
37 L. Rimai and G. A. DeMars, *Phys. Rev.*, 1962, **127**, 702–710.
38 W. Strek, D. Hreniak, G. Boulon, Y. Guyot and R. Pązik, *Opt. Mater.*, 2003, **24**, 15–22.
39 D. Hreniak, W. Strek, J. Amami, Y. Guyot, G. Boulon, C. Goutaudier and R. Pazik, *J. Alloys Compd.*, 2004, **380**, 348–351.
40 C. L. Freeman, J. A. Dawson, H.-R. Chen, J. H. Harding, L.-B. Ben and D. C. Sinclair, *J. Mater. Chem.*, 2011, **21**, 4861–4868.
41 S. Makishima, K. Hasegawa and S. Shionoya, *J. Mol. Struct.*, 1962, **23**, 749–757.
42 C. Cascales, R. Balda, S. García-Revilla, L. Lezama, M. Barredo-Zuriarrain and J. Fernández, *Opt. Express*, 2018, **26**, 16155–16170.

This journal is © The Royal Society of Chemistry 2019